Journal of Magnetism and Magnetic Materials 484 (2019) 212–217

Contents lists available at ScienceDirect

Journal of Magnetism and Magnetic Materials

journal homepage: www.elsevier.com/locate/jmmm

Research articles

# Structure and magnetic properties of $(Sm_{0.9}Zr_{0.1})Fe_{11}Ti$ alloys with $ThMn_{12}$-type structure

D.S. Neznakhin[a], S.V. Andreev[a], M.A. Semkin[a], N.V. Selezneva[a], M.N. Volochaev[b], A.S. Bolyachkin[a], N.V. Kudrevatykh[a], A.S. Volegov[a]

[a] Ural Federal University, 620002 Yekaterinburg, Russia
[b] Kirensky Institute of Physics, Federal Research Center KSC SB RAS, 660036 Krasnoyarsk, Russia

ARTICLE INFO

*Keywords:*
$ThMn_{12}$-type phase
Permanent magnets
Rare earth-lean magnets

ABSTRACT

Rapidly increasing demand for high-energy permanent magnets and volatility of the rear-earth market encourage a search of hard magnetic materials that can compete with those based on the $Nd_2Fe_{14}B$ phase. Sm-Fe compounds with the $ThMn_{12}$-type crystal structure are considered as promising candidates for it. However, their synthesis and achievement of theoretically predicted magnetic properties are still challenging tasks that have not been solved yet. This paper addresses this problem. Its aim was to synthesize and to study magnetic properties of the $(Sm_{0.9}Zr_{0.1})Fe_{11}Ti$ compound with $ThMn_{12}$-type structure. Initially amorphous alloy was obtained by melt spinning and its subsequent heat treatments were performed. Structural and phase transformations of the $(Sm_{0.9}Zr_{0.1})Fe_{11}Ti$ alloy with annealing temperatures were studied along with magnetic properties. For the optimally annealed alloy features of magnetization reversal were discussed and temperature dependences of coercivity and maximum energy product were obtained.

## 1. Introduction

The $RT_{12}$ intermetallic compounds (where R is a rare-earth metal and T is a 3d metal) with the tetragonal $ThMn_{12}$-type crystal structure have been studied since the 1980's [1–4]. This phase is metastable and partial substitutions of T by V, Mo, Nb, Al *etc.* are usually used to form it [5–8]. Depending on the chosen stabilizing element (M), the appropriate number of its atoms varies from 0.5 to 8 per formula unit. The substitution by an element which has no magnetic moment, *e.g.* Ti, leads to magnetization reduction of the $RT_{12-x}M_x$ compound. Therefore, a minimal content of the M element is essential [9]. The $RT_{12-x}M_x$ compound can be modified further by a partial substitution of R element. The efficiency of using Zr for that was demonstrated recently [10–15]. First it allows to reduce the content of a critical rare-earth metal in the compound. Second the substitution of Zr at R sites enhances stability of the $ThMn_{12}$-type phase [10–12] that was confirmed by first-principles studies [15]. Specifically, the Zr substitution resolves the local mismatch in atomic size in the structure. Therefore, an amount of M elements can be additionally decreased due to Zr that improves magnetic properties of the $R_yZr_{1-y}T_{12-x}M_x$ compound [10–12]. Finally, the most common T element – Fe can be partially substituted by Co that positively effects both Curie temperature and magnetization [10–13,16].

Discovery of the $Nd_2Fe_{14}B$ phase reduced the interest to $RT_{12-x}M_x$ compounds for a while since $Nd_2Fe_{14}B$ demonstrated better magnetic properties. However, it was theoretically predicted in Ref. [17] that some compounds of the $ThMn_{12}$-type structure ($NdFe_{12}$; $NdFe_{12}X$ where X = B, N, C; $CeFe_{12}$; $SmFe_{12}N$) may have even a higher maximum energy product $(BH)_{max}$ than the $Nd_2Fe_{14}B$. Also estimated $(BH)_{max}$ of $SmFe_{12}$, $SmFe_{11}Ti$, $SmFe_{12}N$ and $SmFe_{11}TiN$ compounds were close to that for $Nd_2Fe_{14}B$ [17]. In addition, the anisotropy field of $SmFe_{11}Ti$ based alloys exceeds that of $Nd_2Fe_{14}B$ at temperatures above 350 K. These facts stimulated experimental works [10–16,18–20] aimed at the verification of such predictions and synthesis of hard magnetic materials with high magnetic properties. According to these papers, $SmFe_{11}Ti$ based alloys with the $ThMn_{12}$-type structure are the most promising candidates since this compound has a high uniaxial anisotropy as well as a high saturation magnetization [13,19,20].

High coercivity $SmFe_{11}Ti$ based alloys with the $ThMn_{12}$-type structure can be obtained from the amorphous state by an appropriate annealing. This initial state can be realised using melt spinning or mechanical alloying techniques [21,22]. Since this compound has a complex phase diagram and metallurgy, it is important to know how its crystallization is going on with heat treatments and which phase transformations appear. Temperature dependencies of hysteretic magnetic properties for such alloys are of interest also.

*E-mail address:* D.S.Neznakhin@urfu.ru (D.S. Neznakhin).

https://doi.org/10.1016/j.jmmm.2019.04.030
Received 25 September 2018; Received in revised form 9 April 2019; Accepted 9 April 2019
Available online 10 April 2019
0304-8853/ 

Thus, the aim of this paper was to synthesis and to study magnetic properties of the $(Sm_{0.9}Zr_{0.1})Fe_{11}Ti$ alloy with the main phase of $ThMn_{12}$-type structure. Melt spinning was chosen as a synthesis method and a search of the optimal regime of heat treatment maximizing coercivity was performed. Structural and phase transformations in this alloy during annealing at different temperatures were studied in detail along with magnetic properties. For the optimally annealed alloy the temperature dependences of coercivity and maximum energy product were obtained in a wide range.

## 2. Experimental details

Alloys of the $(Sm_{1-y}Zr_y)Fe_{11}Ti$ composition with $y = 0$, 0.1, 0.15 and 0.2 were obtained from chemically pure elements (99.9 %) by induction melting in Ar atmosphere. Next, pieces of alloys were charged into a special quartz crucible with an orifice in the bottom and heated under an Ar atmosphere to melt them. The resulting melts were injected on the rotating surface of a copper wheel which linear velocity was 35 m/s. Strips of alloys were annealed in vacuum for 1 hour at different temperatures from the range of 773–1273 K. Phase compositions of the heat-treated samples were examined by X-ray diffraction (XRD) at Bruker D8 Advance using Cu-$K_\alpha$ radiation. Structural parameters were refined by Rietveld method using Fullprof [23]. Morphology of the samples was studied using transmission electron microscopy (TEM) performed on a Hitachi HT7700 equipped with a STEM system and a Bruker X-Flash 6T/60 EDX detector. Cross-sections of the samples were prepared by a focused ion beam system (FIB) Hitachi FB2100. It was found that the $(Sm_{0.9}Zr_{0.1})Fe_{11}Ti$ alloy had the highest content of the $ThMn_{12}$-type phase among others. Thus, a further research was focused on that alloy.

Temperature dependences of the initial susceptibility were measured using custom-made susceptometer. Magnetic properties of the samples were examined using a vibration sample magnetometer ($H_{max}$ = 25 kOe; room temperature measurements) and using a MPMS XL7 EC ($H_{max}$ = 70 kOe; operating temperature range of 2–800 K).

## 3. Results and discussion

XRD patterns for as-quenched and annealed samples of the $(Sm_{0.9}Zr_{0.1})Fe_{11}Ti$ alloy are shown in Fig. 1. The XRD pattern of as-quenched sample has a wide halo that indicates its X-ray amorphous state. According to the Sm-Fe phase diagram [24], both $Sm_2Fe_{17}$ and α-Fe are equilibrium phases at room temperature for the $SmFe_{12}$ stoichiometric composition. However, $Sm_2Fe_{17}$ phase was not detected in all samples which annealing temperatures ($T_a$) did not exceed 1173 K.

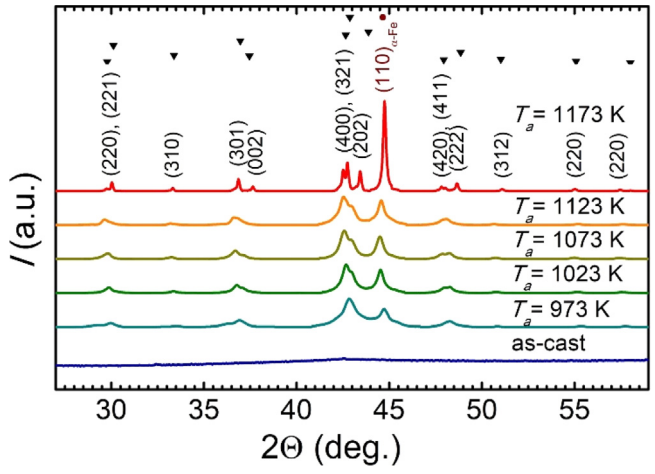


**Fig. 1.** XRD patterns for as-quenched and annealed $(Sm_{0.9}Zr_{0.1})Fe_{11}Ti$ alloy, where $SmFe_{11}Ti$ (▼) [4,25] and α-Fe (●) [26] phases are marked out.

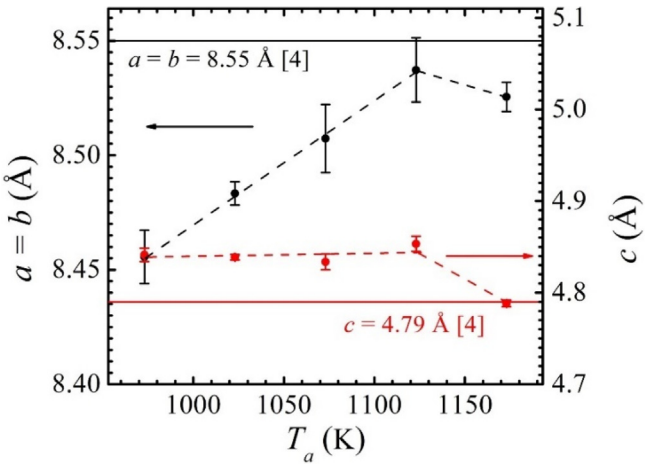


**Fig. 2.** The lattice parameters $a$ and $c$ of $(Sm_{0.9}Zr_{0.1})Fe_{11}Ti$ phase with $ThMn_{12}$-type structure as functions of annealing temperature ($T_a$). Solid lines correspond to data for $SmFe_{11}Ti$ phase from Ref. [4].

Formation of the $ThMn_{12}$-type main phase and α-Fe was registered.

Lattice parameters $a$ and $c$ of the $ThMn_{12}$-type main phase were specified (Fig. 2). The increase of annealing temperature from 973 K to 1123 K led to the $a$ increase from 8.456(12) Å to 8.537(14) Å. Whereas for considered $T_a$ the $c$ parameter was almost the same with value of 4.84(1) Å. For comparison, the lattice parameters of the $SmFe_{11}Ti$ phase obtained for bulk sample are $a$ = 8.55 Å and $c$ = 4.79 Å [4]. At the annealing temperature of 1173 K both $a$ and $c$ decreased to 8.525(6) Å and 4.788(4) Å respectively. The dependencies of $a(T_a)$ and $c(T_a)$ resulted in a variation of the unit cell volume of the $ThMn_{12}$-type phase in the range from 346.1(9) $Å^3$ to 353.7(9) $Å^3$, that is close to reported one of 349.7 $Å^3$ for the $SmFe_{11}Ti$ phase [25]. There was no prominent lattice distortion, which is characterized by the $c/a$ ratio variation, with the annealing temperature. Estimated $c/a$ = 0.57(1) corresponded to the ratio of 0.559 from Ref. [25] within the uncertainties.

The α-Fe lattice parameter varied insignificantly with annealing temperature ($a$ = 2.87(1) Å). The amorphous phase retained up to $T_a$ of 1173 K but its amount gradually decreased with increasing $T_a$. All XRD patterns demonstrated slight reflections of the (Sm,Ti)$Fe_2$ phase overlapping with α-Fe reflections (2θ ≈ 45°). The weight fraction of α-Fe varied from 15 to 30 wt. % in the $T_a$ range of 973–1123 K. Let us note that the most amount of this α-Fe located on the stripes surface. The content of α-Fe reached 50 wt. % after annealing at 1123 K.

Mean grain size ($\langle d \rangle$) of the main $ThMn_{12}$-type phase was estimated using the Scherrer equation [27]. It was of about 20–30 nm at annealing temperatures in the range of 973–1123 K. Grain growth up to 80–100 nm happened during heat treatment at $T_a$ = 1173 K. The mean size of α-Fe grains within samples volume was comparable with that of the main phase grains. The only exceptions were α-Fe grains close to the sample surface which $\langle d \rangle$ was bigger, *e.g.* $\langle d \rangle \approx 300$ nm at $T_a$ = 1073 K. Annealing at higher temperature of 1273 K led to formation of two impurity phases of the $(Sm_{0.9}Zr_{0.1})Fe_{11}Ti$ stoichiometric composition but with $Th_2Zn_{17}$ and $TbCu_7$ structure types [28]. These phases made it complicated to interpret the XRD pattern obtained at $T_a$ = 1273 K.

TEM results are shown in Fig. 3. Well-defined grains were not observed in the as-quenched alloy (Fig. 3(a)) and its electron diffraction represented a wide halo only (inset in Fig. 3(a)). With $T_a$ increasing grains became to grow and their mean size increased: starting from $\langle d \rangle \approx 15$ nm at $T_a$ = 1023 K (Fig. 3(b)) it increased to $\langle d \rangle \approx 28$ nm at $T_a$ = 1073 K (Fig. 3(c)) and then drastic growth up to $\langle d \rangle \approx 430$ nm happened at $T_a$ = 1273 K (Fig. 3(d)). These grain sizes complied well with the estimates from XRD patterns. Grain growth with annealing was also indicated by electron diffraction patterns which contrast, *i.e.* separated rings, was becoming more pronounced at high annealing

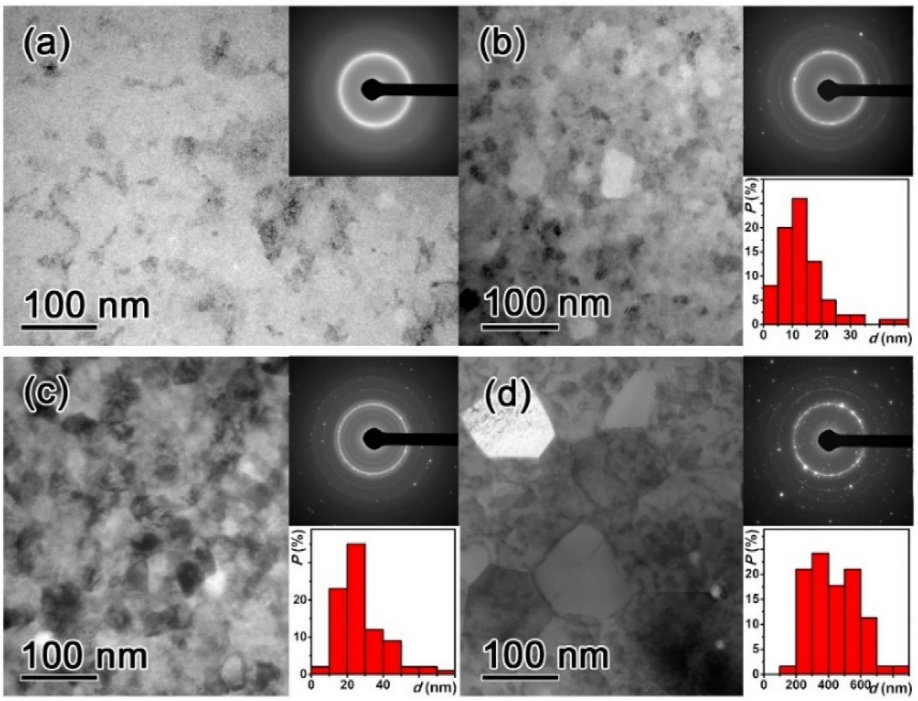


**Fig. 3.** TEM micrographs, electron-diffraction patterns and grain size distributions of the $(Sm_{0.9}Zr_{0.1})Fe_{11}Ti$ alloy in as-quenched state (a) and after annealing at 1023 K (b), 1073 K (c) and 1273 K (d).

temperatures.

According to EDX study, the atomic ratio of the alloy corresponded to the $(Sm_{0.9}Zr_{0.1})Fe_{11}Ti$ composition on volume average with the exception of some small Fe-rich precipitates which look brighter than the main matrix on TEM images (Fig. 4 (a) and (b)). Some of the lasts were depleted of Ti and Sm was almost absent there; atomic distribution identified these regions as the $(Ti,Zr)Fe_2$ phase. Such grains reached a diameter of 200 nm for annealing at 1023 K. However, their volume fraction was insignificant, it did not exceed 3%. Also, a 200–400 nm thick α-Fe layer was observed on the alloy surface at $T_a = 1023$ K (Fig. 4 (a)). α-Fe grains and ones with the element ratio corresponding to $ThMn_{12}$ and $Th_2Zn_{17}$ structure type phases were found at high annealing temperature of 1273 K. There were areas with a (Sm,Zr)/Fe/Ti ratio of 2/53/45 as well as a ratio of 5/72/23. All of that confirms the XRD data about the complicated phase composition of the $(Sm_{0.9}Zr_{0.1})Fe_{11}Ti$ alloy after annealing at $T_a = 1273$ K.

Temperature dependencies of the initial magnetic susceptibility were measured for as-quenched and annealed samples of the $(Sm_{0.9}Zr_{0.1})Fe_{11}Ti$ alloy (Fig. 5). These dependencies allowed to identify magnetically ordered phases formed in the alloys during heat treatments at different $T_a$. The as-quenched $(Sm_{0.9}Zr_{0.1})Fe_{11}Ti$ alloy consisted of the amorphous phase with the Curie temperature ($T_C$) of 345 ± 2 K and a small amount of the α-Fe phase. A peak on the $\chi(T)$

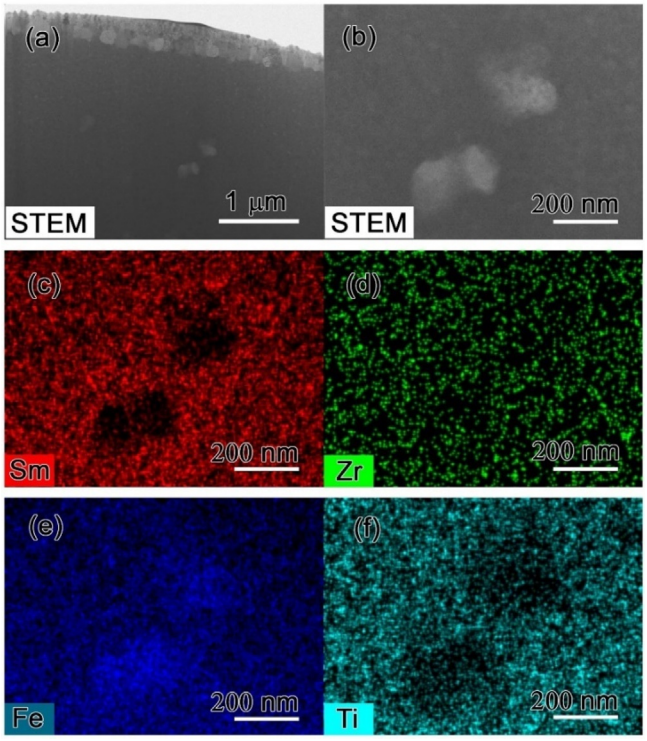


**Fig. 4.** Microstructure and Sm (c), Zr (d), Fe (e) and Ti (f) elemental distributions in $(Sm_{0.9}Zr_{0.1})Fe_{11}Ti$ alloy observed by electron probe micro-analyzer.

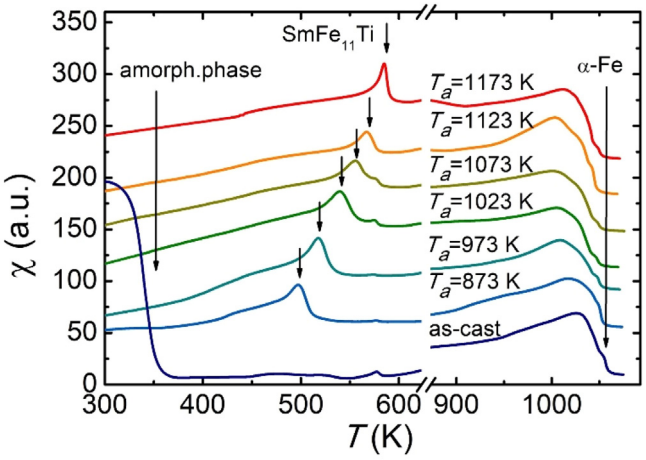


**Fig. 5.** Temperature dependencies of the initial magnetic susceptibility of the $(Sm_{0.9}Zr_{0.1})Fe_{11}Ti$ alloy in as-quenched state and after annealing at different temperatures ($T_a$).

dependence at 583 K, that is close to $T_C$ of the (Ti,Zr)$Fe_2$ phase ($T_C$ = 585 K for $Ti_{0.25}Zr_{0.75}Fe_2$ [29]), was also observed. The presence of the (Ti,Zr)$Fe_2$ phase in a small amount was also detected by the EDX and XRD studies. Let us note that the χ(T) dependence in the temperature range close to $T_C$ of the α-Fe phase had a small flexure. It might be due to α-Fe grains within the volume and the Fe-rich shell of samples which chemical compositions were slightly different from each other.

Susceptibility dependencies of the annealed samples had peaks ascribed to grains of the magnetic phase with the $ThMn_{12}$-type structure. The Curie temperature of this phase increased with increasing annealing temperature (marked with arrows in Fig. 5): it was 513 K at $T_a$ = 873 K and it reached the value of 593 K at $T_a \geq$ 1173 K that was close to the reported $T_C$ = 600 K for the $SmFe_{11}Ti$ phase [4]. Such a remarkable $T_C$ variation during heat treatments might indicate a complex formation of the $(Sm_{0.9}Zr_{0.1})Fe_{11}Ti$ phase with the $ThMn_{12}$-type structure possessing some chemical and structural inhomogeneities. A grain size effect is also able to contribute to the observed feature [30].

Hysteresis loops of the $(Sm_{0.9}Zr_{0.1})Fe_{11}Ti$ alloy annealed at different temperatures were measured. After optimum annealing at $T_a$ = 1073 K during 1 hour, the saturation magnetization ($\sigma_s$) of the alloy was of 107 emu/g and the remanence ($\sigma_r$) was of 70 emu/g. The coercivity ($H_c$) dependence on annealing temperature was a nonmonotonic with a maximum value of 4.6 kOe at $T_a$ = 1073 K (Fig. 6). Thus, there was an optimal heat treatment at this temperature. Corresponding hysteresis loop is shown in the inset of Fig. 6. Its descending branch in a second quadrant had a slight kink at small magnetic fields due to previously mentioned content of soft magnetic phases including amorphous one. Specifically, this kink was caused by α-Fe grains which sizes were much bigger than the domain wall width of 40 nm. These grains had not got efficient exchange coupling with the surrounding, so they started to demagnetize at small magnetic fields with magnetization reversal of the inner part. And on the contrary, small α-Fe grains are exchange-coupled with the main hard magnetic phase. Due to the content of soft magnetic phase and exchange coupling, the increased remanence was observed $\sigma_r/\sigma_s > 0.5$.

Magnetization curves and δ*m*-plots of the $(Sm_{0.9}Zr_{0.1})Fe_{11}Ti$ alloy measured at room temperature are shown in Fig. 7. Samples annealed at 973, 1023 and 1073 K had slight bends on magnetization curves usually attributed to the hysteresis mechanism given either by irreversible magnetization rotation or by domain wall pinning. Since fine grains of the main phase (their mean size was much less than the single domain size of $SmFe_{11}Ti$ phase) and the residual amorphous phase were

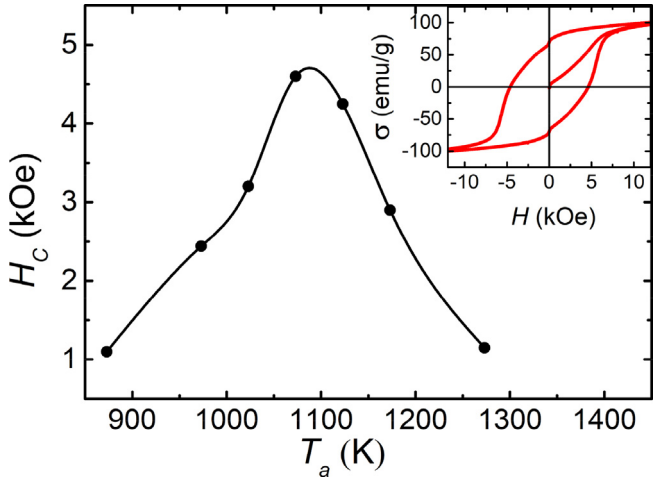


**Fig. 6.** Room-temperature coercivity as a function of annealing temperature ($T_a$). The solid line connecting points is a guide for the eye. The inset presents major hysteresis loop of the $(Sm_{0.9}Zr_{0.1})Fe_{11}Ti$ powder annealed at 1073 K for 1 h.

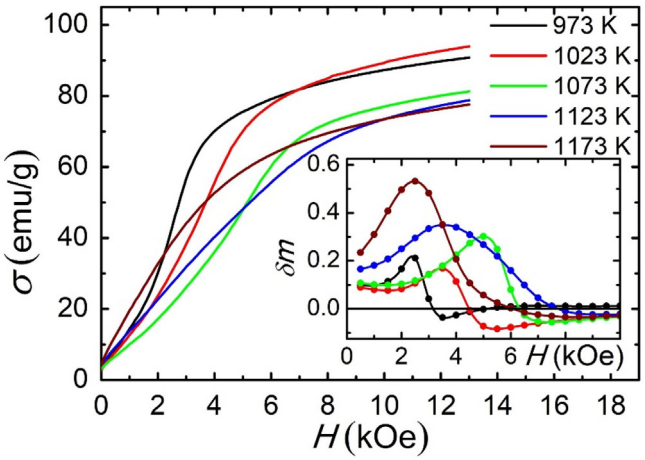


**Fig. 7.** Magnetization curves and δ*m*-plots (inset) of the $(Sm_{0.9}Zr_{0.1})Fe_{11}Ti$ alloy annealed at different temperatures for 1 h.

established at these annealing temperatures both mechanisms are likely to be: irreversible magnetization rotation in grains and domain wall motion in the amorphous phase and some big α-Fe grains with pinning at the interfaces of nanograins [31]. With an increase of $T_a$, their contributions gradually changed towards a predominance of the magnetization rotation accompanied by coercivity increase till its maximum (Fig. 6). At higher annealing temperatures of 1123 K and 1173 K grains became big enough to be in a multidomain state, so the irreversible magnetization rotation was replaced by the nucleation mechanism that decreased coercivity.

The δ*m*-plots [32] of the alloy are shown in the inset of Fig. 7. All of them had a prominent peak, that was located mainly in a positive semiplane ($\delta m > 0$), with a maximum $\delta m_{max}$ at magnetic field close to coercivity. So observed shifts of the peaks were defined by the $H_C(T_a)$ dependence (Fig. 6). Negative part of $\delta m(H)$ plots usually attributed to the effect of demagnetization fields and magnetostatic interactions between grains while the positive one caused by an intergrain exchange interaction of the ferromagnetic type and the higher the strength of this interaction, the bigger $\delta m_{max}$. Let us note, that such approach is valid in some cases of irreversible magnetization rotation [33] and of domain wall pinning [34]. Thus, it can be concluded that among alloys annealed at 973, 1023 and 1073 K the last one had better exchange coupling of grains. But further increase of $\delta m_{max}$ at higher $T_a$ was mainly due to change of the hysteresis type into the nucleation [35]. Nonzero values at small magnetic fields were other features of δ*m*-plots caused by the effect of soft magnetic phases.

Major hysteresis loops of the $(Sm_{0.9}Zr_{0.1})Fe_{11}Ti$ alloy which was annealed at optimal conditions ($T_a$ = 1073 K, 1 hour) were measured within temperature range of 2–575 K. Descending branches of the loops are shown in Fig. 8 (a). Both coercivity and maximum energy product of the alloy were plotted as functions of temperature (Fig. 8 (b)). This coercivity ($H_{C1}$ curve) was underestimated for the hard magnetic phase with the $ThMn_{12}$-type structure due to the effect of the soft magnetic phases. In order to take into account that we suggest the following coercivity evaluation for the hard magnetic phase: coercivity is determined as a position of the dM/dH maximum (Fig. 8 (b); $H_{C2}$ curve) in the vicinity of $H_{C1}$. It can be seen that $H_{C2}$ defined in such a way was higher than $H_{C1}$. As it was previously mentioned, $H_{C1}$ = 4.6 kOe at room temperature. This value is consistent with coercivities of 4.1–5.6 kOe for melt-spun ribbons of the $SmFe_{11}Ti$ alloy that can be found in the literature [21,22,36,37]. Reduced value of $H_{C1}$ is due to the relatively high content of α-Fe phase. However, the proposed estimation of $H_{C2}$ = 5.5 kOe is close to the best coercivity obtained for $SmFe_{11}Ti$ [36].

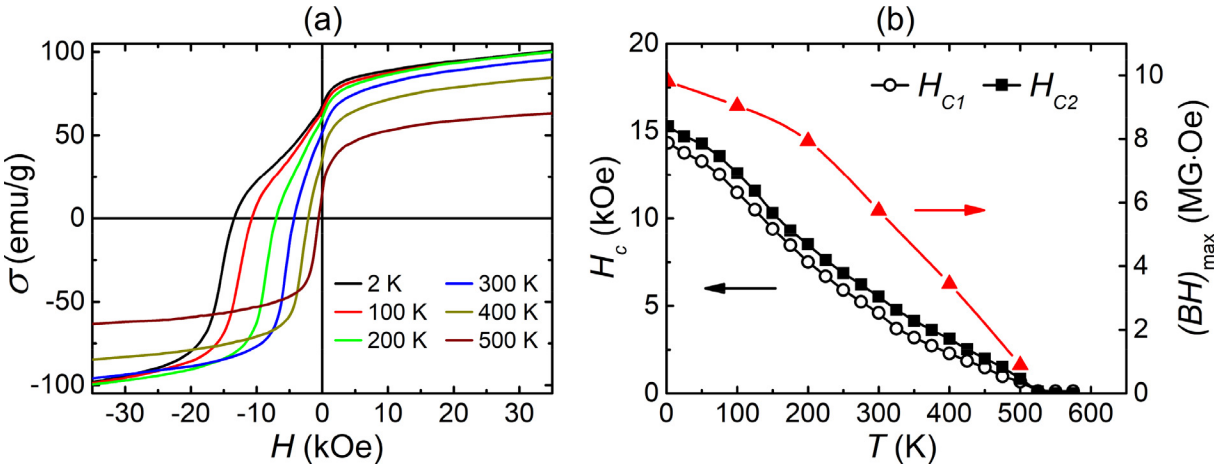


**Fig. 8.** Demagnetization curves of the annealed $(Sm_{0.9}Zr_{0.1})Fe_{11}Ti$ alloy with $ThMn_{12}$-type structure ($T_a$ = 1073 K) measured at different temperatures (a). Temperature dependences of coercivity and maximum energy product for a potential magnet from that alloy (b).

## 4. Conclusion

In this work the $(Sm_{0.9}Zr_{0.1})Fe_{11}Ti$ alloy with the main phase of $ThMn_{12}$-type crystalline structure was obtained by melt spinning and annealing at temperatures in the range of 773–1273 K. Variation of phase composition, lattice parameters of the main phase, microstructure and magnetic properties were studied with annealing temperature ($T_a$). The optimal heat treatment regime that provided the highest coercivity of 4.6 kOe was defined for the alloy: $T_a$ = 1073 K for 1 hour. At these conditions, grains of the main phase with $ThMn_{12}$-type structure were formed with a mean size of 28 nm. Additionally, some amount of α-Fe phase and small content of $(Ti,Zr)Fe_2$ one were observed. For optimally annealed $(Sm_{0.9}Zr_{0.1})Fe_{11}Ti$ alloy the temperature dependences of coercivity and maximum energy product were measured in the range of 2–575 K. There was $(BH)_{max}$ = 5.8 MG·Oe at the room temperature.

However, for $SmFe_{11}Ti$-based alloys, before they become a commercial hard magnetic materials, still some issues have to be solved: the microstructure refinement including better phase purity; further coercivity improvement that can be done by the proper additional treatments including for example grain boundary diffusion processes like in Nd-Fe-B magnets [38] and hard phase nanograins texture formation which probably can be achieved via new HPTC method [39,40].

## Acknowledgement

This work was supported by MES of RF (contract No. 3.6121.2017/8.9) and by Act 211 Government of RF (agreement No. 02.A03.21.0006). TEM was performed in the Center for Shared Use of Federal Research Center KSC SB RAS.

## References

[1] F.J. Cadieu, T.D. Cheung, L. Wickramasekara, S.H. Aly, Magnetic properties of a metastable Sm-Fe phase synthesized by selectively thermalized sputtering, J. Appl. Phys. 55 (1984) 2611–2613.
[2] D.B. De Mooij, K.H.J. Buschow, Some novel ternary $ThMn_{12}$-type compounds, J. Less Common Metals 136 (1988) 207–215.
[3] F.R. De Boer, Y.K. Huang, D.B. De Mooij, K.H.J. Buschow, Magnetic properties of a series of novel ternary intermetallics $(RFe_{10}V_2)$, J. Less Common Metals 135 (1987) 199–204.
[4] A.V. Andreev, A.N. Bogatkin, N.V. Kudrevatykh, S.S. Sigaev, E.N. Tarasov, High-anisotropy rare-earth magnets $RFe_{12-x}M_x$, Phys. Met. Metall. 68 (1) (1989) 68–75.
[5] R. Vert, D. Fruchart, D. Gignoux, Spin reorientations in $RFe_{12-x}Mo_x$ (R = Nd, Tb and 1.5≤x≤1.6) studied from polar magnetisation measurements on oriented powders, J. Magn. Magn. Mater. 242 (2002) 820–822.
[6] B. Garcia-Landa, D. Fruchart, D. Gignoux, J.L. Soubeyroux, R. Vert, Magnetic properties of $RFe_{12-x}Mo_x$ compounds (R = Y, Er), J. Magn. Magn. Mater. 182 (1998) 207–215.
[7] J.L. Wang, C. Marquina, B. García-Landa, M.R. Ibarra, F.M. Yang, G.H. Wu, Magnetovolume effect in $ThMn_{12}$-type Fe-rich $R(Fe, Nb)_{12}$-based compounds, Physica B: Condens. Matter 319 (2002) 73–77.
[8] I. Felner, I. Nowik, Transitions from ferrimagnetism to spin glass behaviour in $YFe_xAl_{12-x}$ (4≤ x≤ 6), J. Magn. Magn. Mater. 54 (1986) 163–164.
[9] H.H. Stadelmaier, F.J. Cadieu, N.C. Liu, Fe-Ti-rare-earth compounds with the tetragonal $Mn_{12}Th$ structure type, Mater. Lett. 6 (3) (1987) 80–81.
[10] T. Kuno, S. Suzuki, K. Urushibata, K. Kobayashi, N. Sakuma, M. Yano, A. Kato, A. Manabe, $(Sm,Zr)(Fe,Co)_{11.0\text{-}11.5}Ti_{1.0\text{-}0.5}$ compounds as new permanent magnet materials, AIP Adv. 6 (2016) 025221.
[11] S. Suzuki, T. Kuno, K. Urushibata, K. Kobayashi, N. Sakuma, K. Washio, et al., A new magnet material with $ThMn_{12}$ structure: $(Nd_{1-x}Zr_x)(Fe_{1-y}Co_y)_{11+z}Ti_{1-z}N_\alpha$ (α = 0.6–1.3), J. Magn. Magn. Mater. 401 (2016) 259–268.
[12] K. Kobayashi, S. Suzuki, T. Kuno, K. Urushibata, N. Sakuma, M. Yano, T. Shouji, A. Kato, A. Manabe, The stability of newly developed (R, Zr)(Fe, $Co)_{12\text{-}x}Ti_x$ alloys for permanent magnets, J. Alloys Compd. 694 (2017) 914–920.
[13] P. Tozman, H. Sepehri-Amin, Y.K. Takahashi, S. Hirosawa, K. Hono, Intrinsic magnetic properties of $Sm(Fe_{1-x}Co_x)_{11}Ti$ and Zr-substituted $Sm_{1-y}Zr_y(Fe_{0.8}Co_{0.2})_{11.5}Ti_{0.5}$ compounds with $ThMn_{12}$ structure toward the development of permanent magnets, Acta Mater. 153 (2018) 354–363.
[14] A.M. Gabay, G.C. Hadjipanayis, Mechanochemical synthesis of magnetically hard anisotropic $RFe_{10}Si_2$ powders with R representing combinations of Sm, Ce and Zr, J. Magn. Magn. Mater. 422 (2017) 43–48.
[15] Y. Harashima, T. Fukazawa, H. Kino, T. Miyake, Effect of R-site substitution and the pressure on stability of $RFe_{12}$: a first-principles study, J. Appl. Phys. 124 (2018) 163902.
[16] A. Urzhumtsev, M. Anikin, E. Tarasov, M. Semkin, M. Cherepkov, N. Kudrevatykh, A. Zinin, V. Moskalev, Effect of alloying elements (Zr, Hf, Co), heat and mechanical treatment conditions on the phase composition and magnetic properties of $SmFe_{11}Ti$ compounds with $ThMn_{12}$ structure, EPJ Web Conf. 185 (2018) 04026.
[17] W. Körner, G. Krugel, C. Elsässer, Theoretical screening of intermetallic $ThMn_{12}$-type phases for new hard-magnetic compounds with low rare earth content, Sci. Rep. 6 (2016) 24686.
[18] I.S. Tereshina, N.V. Kostyuchenko, E.A. Tereshina-Chitrova, Y. Skourski, M. Doerr, I.A. Pelevin, A.K. Zvezdin, M. Paukov, L. Havela, H. Drulis, $ThMn_{12}$-type phases for magnets with low rare-earth content: crystal-field analysis of the full magnetization process, Sci. Rep. 8 (2018) 3595.
[19] A.M. Gabay, R. Cabassi, S. Fabbrici, F. Albertini, G.C. Hadjipanayis, Structure and permanent magnet properties of $Zr_{1-x}R_xFe_{10}Si_2$ alloys with R = Y, La, Ce, Pr and Sm, J. Alloys Compd. 683 (2016) 271–275.
[20] A. Martin-Cid, D. Salazar, A.M. Schönhöbel, J.S. Garitaonandia, J.M. Barandiaran, G.C. Hadjipanayis, Magnetic properties and phase stability of tetragonal $Ce_{1-x}Sm_xFe_9Co_2Ti$ 1:12 phase for permanent magnets, J. Alloys Compd. 749 (2018) 640–644.
[21] T. Saito, H. Miyoshi, D. Nishio-Hamane, Magnetic properties of Sm–Fe–Ti nanocomposite magnets with a $ThMn_{12}$ structure, J. Alloys Compd. 519 (2012) 144–148.
[22] H. Wuest, L. Bommer, A.M. Huber, D. Goll, T. Weissgaerber, B. Kieback, Preparation of nanocrystalline $Ce_{1-x}Sm_x(Fe, Co)_{11}Ti$ by melt spinning and mechanical alloying, J. Magn. Magn. Mater. 428 (2017) 194–197.
[23] J. Rodriguez-Carvajal, Recent advances in magnetic structure determination by neutron powder diffraction, Physica B 192 (1993) 55–69.
[24] O. Kubaschewski, Iron—Binary Phase Diagrams, Springer Science & Business Media, 2013.
[25] L.X. Liao, Z. Altounian, D.H. Ryan, Structure and magnetic properties of $RFe_{11}TiN_x$ (R = Y, Sm, and Dy), J. Appl. Phys. 70 (1991) 6006–6008.
[26] M. Reibold, A.A. Levin, D.C. Meyer, P. Paufler, W. Kochmann, Microstructure of a damascene sabre after annealing, Int. J. Mater. Res. 97 (2006) 1172–1182.
[27] P. Scherrer, Estimation of the size and internal structure of colloidal particles by means of röntgen, Göttinger Nachrichten Gesell. 2 (1918) 98.

[28] D. Wang, S.H. Liou, P. He, D.J. Sellmyer, G.C. Hadjipanayis, Y. Zhang, $SmFe_{12}$ and $SmFe_{12}N_x$ films fabricated by sputtering, J. Magn. Magn. Mater. 124 (1993) 62–68.
[29] E. Piegger, R.S. Craig, Structural and magnetic characteristics of $TiFe_2$–$ZrFe_2$ and $ZrCo_2$–$ZrFe_2$ alloys, J. Chem. Phys. 39 (1) (1963) 137–145.
[30] K. Binder, Statistical mechanics of finite three-dimensional Ising models, Physica 62 (1972) 508–526.
[31] G. Huang, X. Li, L. Lou, Y. Hua, G. Zhu, M. Li, H.-T. Zhang, J. Xiao, B. Wen, M. Yue, X. Zhang, Engineering bulk, layered, multicomponent nanostructures with high energy density, Small 14 (2018) 1800619.
[32] P.E. Kelly, K. O'Grady, P.I. Mayo, R.W. Chantrell, Switching mechanisms in cobalt-phosphorus thin films, IEEE Trans. Magn. 25 (5) (1989) 3881–3883.
[33] E.P. Wohlfarth, Relations between different modes of acquisition of the remanent magnetization of ferromagnetic particles, J. Appl. Phys. 29 (1958) 595–596.
[34] P. Gaunt, G.C. Hadjipanayis, C. Ng, Remanence relationships and domain wall pinning in ferromagnets, J. Magn. Magn. Mater. 54–57 (1986) 841842.
[35] R.W. Gao, D.H. Zhang, W. Li, X.M. Li, J.C. Zhang, Hard magnetic property and δM (H) plot for sintered NdFeB magnet, J. Magn. Magn. Mater. 208 (2000) 239–243.
[36] Y. Wang, G.C. Hadjipanayis, A. Kim, N.C. Liu, D.J. Sellmyer, Magnetic and structural studies in Sm-Fe-Ti magnets, J. Appl. Phys. 67 (9) (1990) 4954–4956.
[37] J. Wecker, M. Katter, L. Schultz, High coercivity in Sm-Fe-Ti alloys by rapid solidification, Mater. Sci. Eng. A 133 (1991) 147–150.
[38] R. Madugundo, D. Salazar-Jaramillo, J.M. Barandiaran, G.C. Hadjipanayis, High coercivity in rare-earth lean nanocomposite magnets by grain boundary infiltration, J. Magn. Magn. Mater. 400 (2016) 300–303.
[39] X. Li, L. Lou, W. Song, G. Huang, F. Hou, Q. Zhang, H.-T. Zhang, J. Xiao, B. Wen, X. Zhang, Novel bimorphological anisotropic bulk nanocomposite materials with high energy products, Adv. Mater. 29 (2017) 1606430.
[40] X. Li, L. Lou, W. Song, Q. Zhang, G. Huang, Y. Hua, H.-T. Zhang, J. Xiao, B. Wen, X. Zhang, Controllably manipulating three-dimensional hybrid nanostructures for bulk nanocomposites with large energy products, Nano Lett. 17 (2017) 2985–2993.